Computational Hypersonic Aerodynamics with Emphasis on Earth Reentry Capsules

Mihai Leonida NICULESCU*,[1], Maria Cristina FADGYAS[1],
Marius Gabriel COJOCARU[1], Mihai Victor PRICOP[1],
Mihaita Gilbert STOICAN[1], Dumitru PEPELEA[1]

*Corresponding author
[1]INCAS − National Institute for Aerospace Research "Elie Carafoli",
Flow Physics Department, Numerical Simulation Unit,
B-dul Iuliu Maniu220, Bucharest 061126, Romania
niculescu.mihai@incas.ro*, fadgyas.maria@incas.ro, cojocaru.gabriel@incas.ro,
pricop.victor@incas.ro, stoican.gilbert@incas.ro, pepelea.dumitru@incas.ro

DOI: 10.13111/2066-8201.2016.8.3.5

Received: 10 June 2016/ Accepted: 20 July 2016/ Published: September 2016
© Copyright 2016, INCAS. This is an open access article under the CC BY-NC-ND license (http://creativecommons.org/licenses/by-nc-nd/4.0/)

4th International Workshop on Numerical Modelling in Aerospace Sciences, NMAS 2016*, 11-12 May 2016, Bucharest, Romania, (held at INCAS, B-dul Iuliu Maniu 220, sector 6)*
Section 2 – Flight dynamics simulation

Abstract: *The temperature in the front region of a hypersonic vehicle nose can be extremely high, for example, reaching approximately 11 000 K at a Mach number of 36 (Apollo reentry) due to the bow shock wave. In this case, accurate prediction of temperature behind the shock wave is necessary in order to precisely estimate the wall heat flux. A better prediction of wall heat flux leads to smaller safety coefficient for thermal shield of space reentry vehicle; therefore, the size of thermal shield decreases and the payload could increase. However, the accurate prediction of temperature behind the bow shock wave implies the use of a precise chemical model whose partial differential equations are added to Navier-Stokes equations. This second order partial differential system is very difficult to be numerically integrated. For this reason, the present paper deals with the computational hypersonic aerodynamics with chemical reactions with the aim of supporting Earth reentry capsule design.*

Key Words*: Hypersonic flow, bow shock wave, dissociation chemical reactions, AUSM$^+$-up scheme, Earth reentry capsule.*

1. INTRODUCTION

Today hypersonic vehicles are commonplace. They include missiles, launch vehicles and reentry bodies such as space shuttles and reentry capsules. In the front region of these vehicles, a very strong shock wave appears that generates a huge increase of temperature. Fortunately, the endothermic chemical reactions of molecular oxygen and nitrogen dissociation and of ionization and plasma formation appear in and behind the bow shock wave. A lot of heat is absorbed due to these chemical reactions; therefore, the temperature decreases impressively that leads to much smaller wall heat flux, i.e. the task of thermal shield is alleviated. Unfortunately, the kinetics of these reactions is very complex, not very

well understood and requires huge computational resources. For this reason, the present paper focuses on chemical reactions that occur at the Earth reentry of space vehicles such as capsules and shuttles.

2. GOVERNING EQUATIONS

The classic governing equations for hypersonic gas dynamics in ***thermal equilibrium*** are the Navier-Stokes equations at which, one adds the transport equations of species Y_i that appear/disappear due to the chemical reactions [1, 2] (a careful reader should firstly read [1] and after that [2]):

$$\frac{\partial U}{\partial t} + \frac{\partial (F_x - G_x)}{\partial x} + \frac{\partial (F_y - G_y)}{\partial y} + \frac{\partial (F_z - G_z)}{\partial z} = S \tag{1}$$

where the conservative variable vector U, convective flux F, diffusive flux G and source term S are given by

$$U = \begin{pmatrix} \rho \\ \rho u \\ \rho v \\ \rho w \\ \rho E \\ \rho Y_i \end{pmatrix}, \quad F_x = \begin{pmatrix} \rho u \\ \rho u^2 + p \\ \rho uv \\ \rho uw \\ \rho uH \\ \rho uY_i \end{pmatrix}, \quad F_y = \begin{pmatrix} \rho v \\ \rho vu \\ \rho v^2 + p \\ \rho vw \\ \rho vH \\ \rho vY_i \end{pmatrix}, \quad F_z = \begin{pmatrix} \rho w \\ \rho wu \\ \rho wv \\ \rho w^2 + p \\ \rho wH \\ \rho wY_i \end{pmatrix} \tag{2}$$

$$G_x = \begin{pmatrix} 0 \\ \tau_{xx} \\ \tau_{xy} \\ \tau_{xz} \\ u\tau_{xx} + v\tau_{xy} + w\tau_{xz} + k\dfrac{\partial T}{\partial x} + \rho \displaystyle\sum_{i=1}^{N} h_i D_{i\ mixture} \dfrac{\partial Y_i}{\partial x} \\ \rho D_{i\ mixture} \dfrac{\partial Y_i}{\partial x} \end{pmatrix} \tag{3}$$

$$G_y = \begin{pmatrix} 0 \\ \tau_{yx} \\ \tau_{yy} \\ \tau_{yz} \\ u\tau_{yx} + v\tau_{yy} + w\tau_{yz} + k\dfrac{\partial T}{\partial y} + \rho \displaystyle\sum_{i=1}^{N} h_i D_{i\ mixture} \dfrac{\partial Y_i}{\partial y} \\ \rho D_{i\ mixture} \dfrac{\partial Y_i}{\partial y} \end{pmatrix} \tag{4}$$

$$G_z = \begin{pmatrix} 0 \\ \tau_{zx} \\ \tau_{zy} \\ \tau_{zz} \\ u\tau_{zx} + v\tau_{zy} + w\tau_{zz} + k\dfrac{\partial T}{\partial z} + \rho\sum_{i=1}^{N} h_i D_{i\ mixture}\dfrac{\partial Y_i}{\partial z} \\ \rho D_{i\ mixture}\dfrac{\partial Y_i}{\partial z} \end{pmatrix} \tag{5}$$

$$S = \begin{pmatrix} 0 \\ 0 \\ 0 \\ 0 \\ -\sum_{i=1}^{N}\left[h_i^{formation\ \ T_{ref}} - cp_i\left(T_{ref}\right)\cdot T_{ref}\right]\cdot \omega_i \\ \omega_i \end{pmatrix} \tag{6}$$

The viscous stresses τ are computed according to Stokes hypothesis for a Newtonian fluid:

$$\begin{aligned} &\tau_{xx} = \frac{2}{3}\mu\left(2\frac{\partial u}{\partial x} - \frac{\partial v}{\partial y} - \frac{\partial w}{\partial z}\right),\ \ \tau_{yy} = \frac{2}{3}\mu\left(2\frac{\partial v}{\partial y} - \frac{\partial u}{\partial x} - \frac{\partial w}{\partial z}\right), \\ &\tau_{zz} = \frac{2}{3}\mu\left(2\frac{\partial w}{\partial z} - \frac{\partial u}{\partial x} - \frac{\partial v}{\partial y}\right), \\ &\tau_{xy} = \tau_{yx} = \mu\left(\frac{\partial u}{\partial y} + \frac{\partial v}{\partial x}\right),\ \ \tau_{xz} = \tau_{zx} = \mu\left(\frac{\partial u}{\partial z} + \frac{\partial w}{\partial x}\right),\ \ \tau_{yz} = \tau_{zy} = \mu\left(\frac{\partial w}{\partial y} + \frac{\partial v}{\partial z}\right) \end{aligned} \tag{7}$$

To close the above second order partial differential system, it is necessary to add supplementary constitutive (closure) relations:

- The temperature behind the bow shock wave is huge (of order of thousands *K*) while the pressure is relatively low (usually, it does not exceed 1 bar); therefore, the equation of ideal gas is valid:

$$p = \rho R^0 T\sum_{i=1}^{N}\frac{Y_i}{W_i},\ \ R^0 = 83143\frac{J}{kmol\cdot K}\ ,\ \ N = number\ of\ \ chemical\ species \tag{8}$$

- Because the pressure is relatively low even behind the bow shock wave (usually, it does not exceed 1 bar); one can use the hypothesis of a *calorically perfect gas for chemical species*:

$$h_i = h_i(T) = c_{p_i}(T)\cdot T \tag{9}$$

- For dynamic viscosity of species μ_i, one can use the kinetic theory of gases or Sutherland law with 3 coefficients:

$$\mu_i(T) = \mu_{0_i} \cdot \left(\frac{T}{T_{0_i}}\right)^{1.5} \cdot \frac{T_{0_i} + S_i}{T + S_i} \tag{10}$$

- For thermal conductivity of species k_i, one can use the kinetic theory of gases
- For the mass diffusivity of chemical species i in the mixture $D_{i\ mixture}$, we should use the kinetic theory of gases because one cannot anymore use the assumption that $D_{i\ mixture}$ is constant like in the burning of hydrocarbons where one can assume that $D_{i\ mixture} \approx 2.88$ E-5 m^2/s
- The flow is laminar; therefore, the chemistry is given by Arrhenius law:

$$\sum_{i=1}^{N} \nu_{ij}^{'} M_i \xrightarrow{k_f} \sum_{i=1}^{N} \nu_{ij}^{''} M_i \qquad N = number\ of\ \ chemical\ species,$$

$$j = 1..number\ of\ \ chemical\ reactions$$

$$\omega_i = W_i \sum_{j=1}^{number\ of\ \ reactions} \left[\left(\nu_{ij}^{''} - \nu_{ij}^{'}\right) \Gamma_j k_{f_j} \prod_{i=1}^{N} \left(\frac{X_i p}{R^0 T}\right)^{\nu_{ij}^{'}} \right] \tag{11}$$

where

$$X_i = Y_i \cdot \frac{W}{W_i}, \quad \frac{1}{W} = \sum_{i=1}^{N} \frac{Y_i}{W_i}, \qquad k_{f_j} = A_j T^{\beta_j} e^{-\frac{E_j}{R^0 T}} \quad - \quad Arrhenius\ law$$

- The pre-exponential factor A, temperature exponent β, activation energy E and third body efficiency Γ are determined experimentally. Unfortunately, they are not constant over the whole range of temperature and pressure. For their experimental determination, one uses typical reentry scenarios for capsules and space shuttles. In this paper, the values given by Park in [3] are used:

Table 1. a) – Forward reactions rate parameters based on the Park '89 model [3] in the Viviani – Pezzella variant [2]

No.	Reaction	$A_{f,r}$ [$K^{-\beta_{f,r}}$/s]	$\beta_{f,r}$	E_r [J/kmol]	3rd body efficiency Γ
1.	$O_2+M \rightarrow 2O+M$	1.00E19	-1.5	4.947E8	$O_2=N_2=NO=0.2$; $O=N=1$
2.	$N_2+M \rightarrow 2N+M$	3.00E19	-1.6	9.412E8	$O_2=N_2=NO=0.233$; $O=N=1$
3.	$NO+M \rightarrow N+O+M$	1.10E14	0	6.277E8	$O_2=N_2=0.05$; $O=N=NO=1$
4.	$NO+O \rightarrow O_2+N$	2.40E6	1	1.598E8	-
5.	$N_2+O \rightarrow NO+N$	1.80E11	0	3.193E8	-

Table 1. b) – Forward reactions rate parameters based on the Park '89 model [3] in the Carandente variant [4]

No.	Reaction	$A_{f,r}$ [$K^{-\beta_{f,r}}$/s]	$\beta_{f,r}$	E_r [J/kmol]	3rd body efficiency Γ
1.	$O_2+M \rightarrow 2O+M$	2.00E18	-1.5	4.947E8	$O_2=N_2=NO=1$; $O=N=5$
2.	$N_2+M \rightarrow 2N+M$	7.00E18	-1.6	9.412E8	$O_2=N_2=NO=1$; $O=N=4.28$
3.	$NO+M \rightarrow N+O+M$	5.00E12	0	6.277E8	$O_2=N_2=1$; $O=N=NO=22$

4.	$NO+O \rightarrow O_2+N$	2.40E6	1	1.598E8	-
5.	$N_2+O \rightarrow NO+N$	1.80E11	0	3.193E8	-

Table 2. a) – Stoichiometric coefficients of reactants for the Park '89 model [3]

Number of species	Number of reaction				
ν'	j=1	j=2	j=3	j=4	j=5
i=1:O_2	1	0	0	0	0
i=2:N_2	0	1	0	0	1
i=3:NO	0	0	1	1	0
i=4:O	0	0	0	1	1
i=5:N	0	0	0	0	0

Table 2. b) – Stoichiometric coefficients of products of reaction for the Park '89 model [3]

Number of species	Number of reaction				
ν''	j=1	j=2	j=3	j=4	j=5
i=1:O_2	0	0	0	1	0
i=2:N_2	0	0	0	0	0
i=3:NO	0	0	0	0	1
i=4:O	2	0	1	0	0
i=5:N	0	2	1	1	1

It is worthwhile to notice that the ***units of pre-exponential factor A given in [2, 4] are wrong***. In order to properly determine the units of pre-exponential factor A, we should take into account the reaction rate ω_i [kg/m^3.s], molecular weight W_i [kg/kmol] and molar concentration $(X_i.p)/(R^0.T)$ [kmol/m^3]. A careful reader should consult [5].

$$[\mathrm{A}_{\mathrm{f,r}}]_{SI} = \left[\left(\frac{m^3}{kmol} \right)^{1-1} \cdot \frac{K^{-\beta_{f,r}}}{s} \right] = \left[\frac{K^{-\beta_{f,r}}}{s} \right] \tag{12}$$

One clearly sees that the pre-exponential factor A of reactions of dissociation of molecular oxygen O_2 and nitrogen N_2 is much bigger than the pre-exponential factor A of reactions of formation/destruction of nitrogen-oxide NO.

For this reason, it is possible to consider only the reactions of dissociation of molecular oxygen and nitrogen and to neglect the formation/destruction of nitrogen-oxide NO. This decreases significantly the computational effort and increases impressively the robustness of numerical algorithm.

It is possible to rewrite those 5 chemical reactions given in Table 1 and Table 2 without the third body efficiency Γ; i.e. it is possible to write 17 chemical reactions without the third body efficiency.

From the mathematical point of view, these two formulations are equivalent but they are not equivalent from the numerical point of view because the last formulation requires the computation of 17 exponentials instead of five, which is expensive from the computational point of view.

In the hypersonic gas dynamics, one prefers to use the kinetic theory of gases as much as possible. For this reason, ***the rate exponents are the stoichiometric coefficients of reactants ν'_{ij} (see Eq. 11)*** while for the common applications (for example for the burning of hydrocarbons), the rate exponents are determined experimentally.

It is preferable to use the formation enthalpy of species i $h_i^{formation\ Tref}$ at reference temperature T_{ref} of 0 K in order to simplify the expression of source term in the energy equation, see Eq. 6.

Unfortunately, the formation enthalpy of species is usually given at common reference temperatures, for example at T_{ref} of 298.15 K.

From the mathematical and numerical point of view, Tables 1. a) and 1. b) are equivalent but they are different from the chemical interpretation.

For example, at reaction 1, Table 1. a) shows that molecular oxygen O_2, molecular nitrogen N_2 and nitrogen-oxide NO are inhibitors while Table 1. b) indicates that atomic oxygen O and nitrogen N are catalysts.

3. NUMERICAL SIMULATIONS AND RESULTS

The 2D and 3D numerical simulations were computed with commercial code Ansys Fluent over a sphere-cone reentry capsule whose geometry is given in [6].

The convective flux was discretized with AUSM$^+$-up scheme [7] because this scheme seems to be the best for hypersonic gas dynamics [8, 9]. Due to carbuncle phenomenon, the convective flux was discretized with the original AUSM$^+$-up scheme [7], which is a first order upwind scheme.

To speed up convergence to the steady-state solution, the initialization was made with FMG (Full MultiGrid) technique [10] with thousands of cycles.

Due to its robustness, we have preferred the implicit formulation rather than the explicit one. Due to carbuncle phenomenon, the calculation was made with the solution steering technique [11].

A very useful feature of this technique consists in automatic decrease of CFL number when the divergence is detected.

Furthermore, severe limitations of minimum and maximum pressure and temperature were made, in order to speed up convergence and avoid divergence due to carbuncle phenomenon.

Moreover, the relaxation to chemical equilibrium model [10] was employed to mitigate the unwanted carbuncle phenomenon. The 3D grid has about 3.4 millions of mixed cells (tetrahedrons and hexahedrons), see Fig. 1.

The hexahedral cells were used only near the capsule while the tetrahedral cells were employed in rest of computational domain to increase the numerical (artificial) viscosity in order to diminish the spurious numerical oscillations. A symmetry plane was introduced in order to decrease the computational effort.

From Fig. 2 one clearly sees that the pressure coefficient at stagnation point is nearly 2, which is in concordance with the Newtonian impact flow theory [2]. The flow over capsule in symmetry plane is given in Fig. 3.

One clearly sees the bow shock wave and the wake region behind the capsule. The bow shock wave is smeared at the end of computational domain because the mesh is coarse at the end of computational domain.

The formation/destruction of species is given in Figs. 4 and 5. The molecular oxygen O_2 dissociates completely behind the bow shock wave near the stagnation point region while the molecular nitrogen N_2 dissociates partially, which indicates that the ionization does not occur. The maximal concentration of nitrogen-oxide NO does not exceed 2%; therefore, the reactions of formation/destruction of this very unstable species could be neglected.

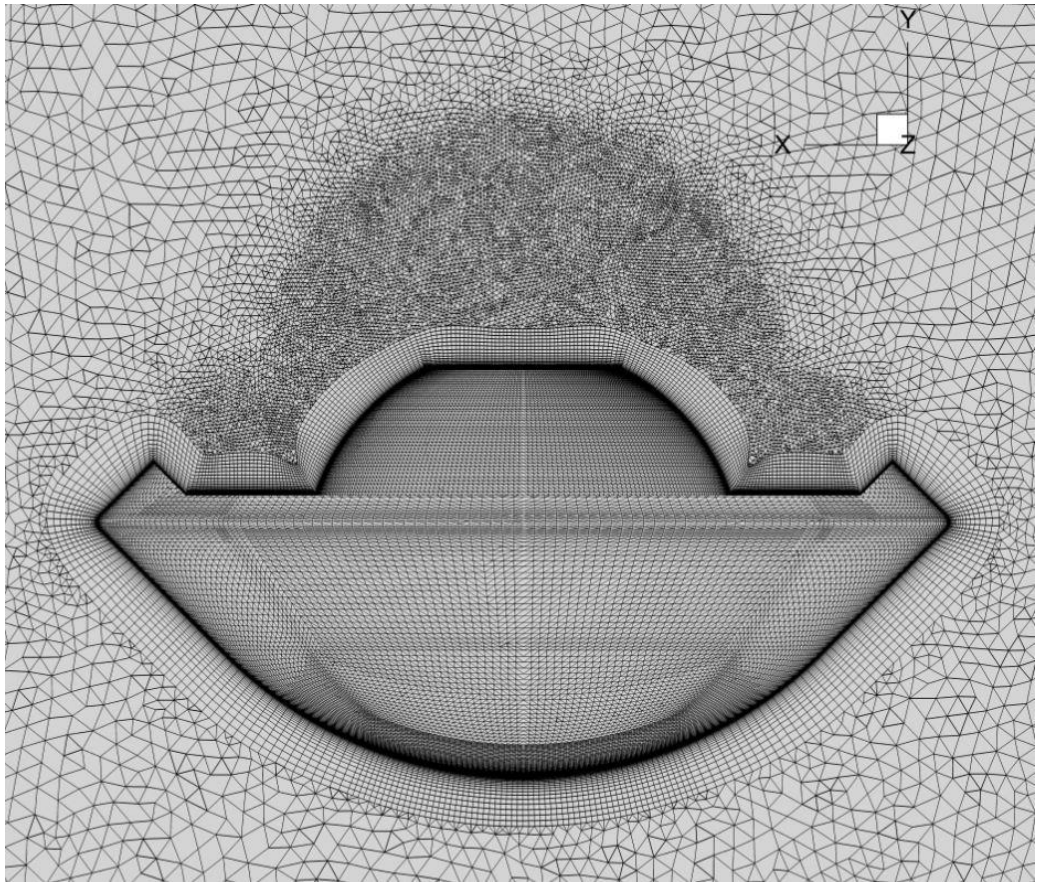

Fig. 1 – Detail of the grid near the capsule

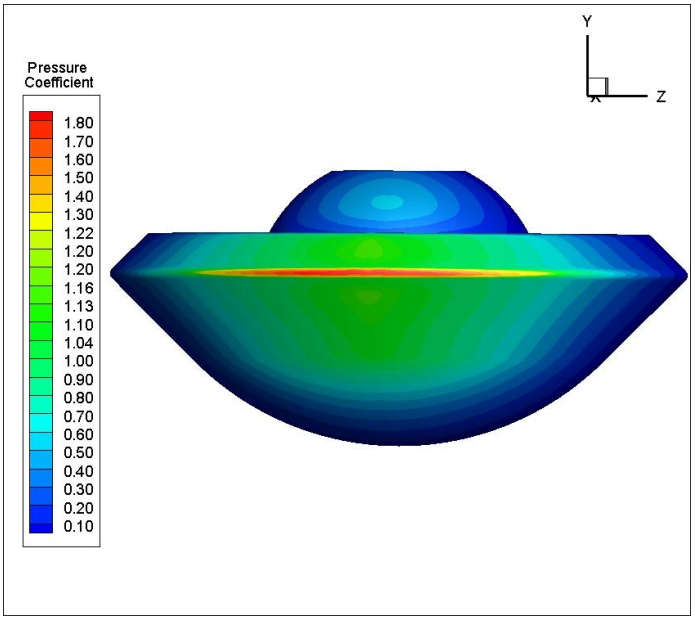

Fig. 2 – Pressure coefficient for an angle of attack of 90^{o} over capsule at M_{∞}=20, H=50 [km]

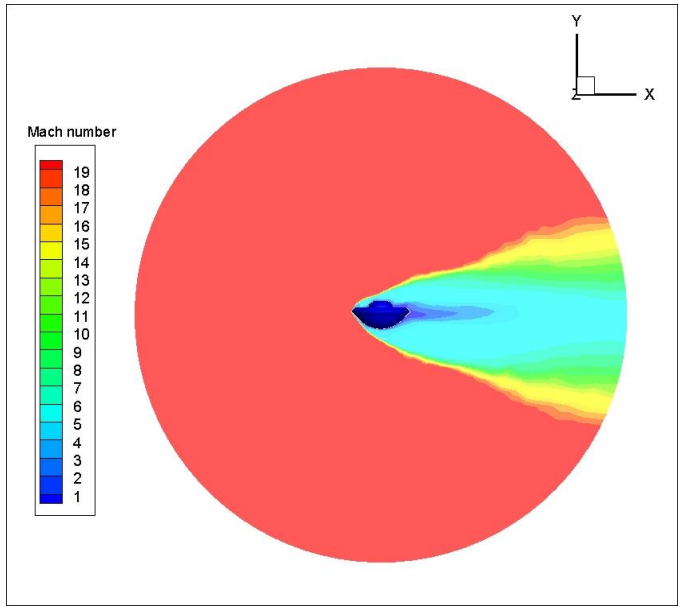

Fig. 3 – Mach number for an angle of attack of 90^o over capsule at M_∞=20, H=50 [km]

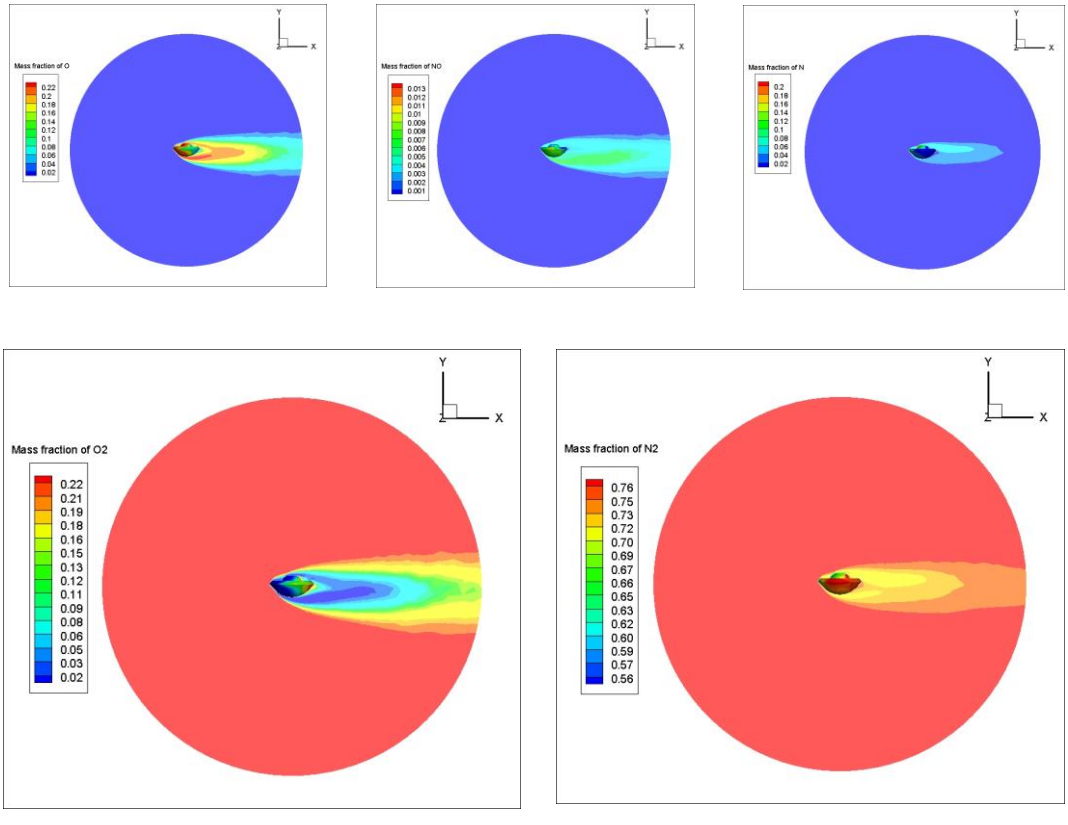

Fig. 4 – Species mass fraction for an angle of attack of 90^o over capsule at M_∞=20, H=50 [km]

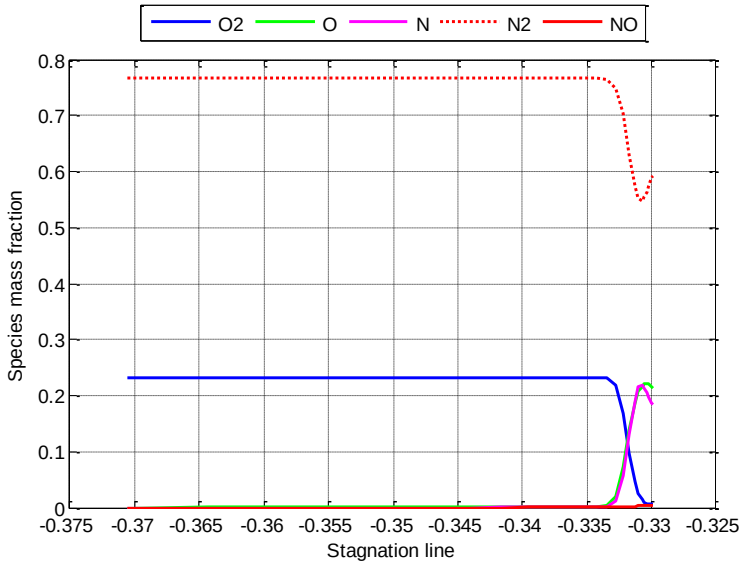

Fig. 5 – Species mass fraction along the stagnation line for an angle of attack of 90° at M_∞=20, H=50 [km]

The position of the shock wave given by CFD results, see Fig. 5, should be compared with the analytical relations, such as those given in [2, 12, 13]:

$$\frac{\Delta}{R_N} = 0.78\frac{\rho_\infty}{\rho_2} \tag{13}$$

$$\frac{\Delta}{R_N} = 0.143 \cdot e^{\frac{3.24}{M_\infty^2}} \tag{14}$$

where Δ is the stand-off distance between bow shock wave and body, R_N is the nose radius of body and ρ_2 is the density behind the shock wave.

4. CONCLUSIONS

Further work is necessary to be done in order to increase the accuracy of numerical simulation and to mitigate the spurious numerical oscillations (carbuncle phenomenon). Practically, there are 2 main ways. The first way consists in increasing the numerical accuracy using Ansys Fluent. Firstly, the specific heats at constant pressure of species c_{pi} should be functions of temperature at least until 10 000 K because now, they are functions of temperature until 5 000 K.

Secondly, we should renounce at the hypothesis of thermal equilibrium that implies the writing of partial differential equations for vibrational temperatures of species through User-Defined Functions (UDFs) [14].

The second way consists in developing an in-house code for hypersonic flows. This gives us a better flexibility in the choice of values of a numerical scheme tuning parameters, of primitive or conservative variables reconstruction and limiters. Some progress was made in this direction and we consider to publish soon some results.

REFERENCES

[1] T. J. Chung, *Computational fluid dynamics*, Cambridge University Press, pp. 724-733, 2002.
[2] A. Viviani and G. Pezzella, *Aerodynamic and aerothermodynamic analysis of space mission vehicles*, Springer International Publishing, pp. 64-72, 112-114, 385-392, 2015.
[3] C. Park, A review of Reaction rates in high temperature air, *AIAA paper*, vol. **89**, 1989.
[4] V. Carandente, *Aerothermodynamic and mission analyses of deployable aerobraking Earth re-entry systems*, Ph. D. Thesis, University of Naples "Federico II", pp. 24-29, 2014.
[5] * * * Ansys CFX, *Solver Theory Guide*, release 16, pp. 213-214, 2015.
[6] V. Carandente, R. Savino, M. Iacovazzo and C. Boffa, Aerothermal analysis of a sample-return reentry capsule, *FDMP*, vol. **9**, no. 4, pp. 461-484, 2013.
[7] M.-S. Liou, A sequel to AUSM, Part II: AUSM$^+$-up for all speeds, *Journal of Computational Physics*, vol. **214** (1), pp. 137-170, 2006.
[8] K. Kitamura and E. Shima, Towards shock-stable and accurate hypersonic heating computations: A new pressure flux for AUSM-family schemes, *Journal of Computational Physics*, vol. **245**, pp. 62-83, 2013.
[9] K. Kitamura, Assessment of SLAU2 and other flux functions with slope limiters in hypersonic shock-interaction heating, *Computers & Fluids*, vol. **129**, pp. 134-145, 2016.
[10] * * * Ansys Fluent, *Theory Guide*, release 16, pp. 191-192, 677-679, 2015.
[11] * * * Ansys Fluent, *Users Guide*, release 16, pp. 1602-1607, 2015.
[12] F. S. Billig, Shock-wave shapes around spherical-and cylindrical-nosed bodies, *Journal of Spacecraft and Rockets*, vol. **4**, 1967.
[13] E. Papadopoulou, *Numerical simulations of the Apollo 4 reentry trajectory*, Master Thesis, Aristotle University of Thessaloniki and École Polytechnique Fédérale de Lausanne, pp. 8, 2013.
[14] * * * Ansys Fluent, *Customization Manual*, release 16, 2015.